Electron gas cooling in Ag nanoparticles on graphite

M. Merschdorf, W. Pfeiffer, S. Voll, and G. Gerber
Physikalisches Institut, Universität Würzburg, D-97074 Würzburg, Germany
(Received 22 May 2003; published 16 October 2003)

The electron energy distribution in supported Ag nanoparticles is measured using multiphoton photoemission. The variation of the photoemission spectrum with temperature allows us to measure the electron gas temperature in the particles. Time-resolved photoemission reveals an electron gas cooling rate of about 0.7 ps^{-1} that varies little with size (1.5–4.5 nm) and is reduced by a factor of about 2 in comparison to bulk Ag and embedded nanoparticles. The modified relaxation behavior for supported nanoparticles is attributed to the different role of excited electron transfer.

DOI: 10.1103/PhysRevB.68.155416 PACS number(s): 78.67.Bf, 73.22.−f, 78.47.+p

Controlling the surface composition and structure on a nanometer scale allows us to prepare surfaces with custom-made properties. This is possible since the properties of nanoparticles are influenced by their size, shape, and the coupling to the substrate. Supported nanoparticles retain some of the properties of isolated particles and are therefore of great interest, e.g., to optimize catalytic surface reactions.[1] Although the influence of particle size and electronic properties on the catalytic activity is known,[2,3] a complete understanding of the mechanisms is missing. In particular, the influence of the electronic structure of nanoparticles on their catalytic activity is not well understood. In addition to the electronic structure, the relaxation behavior of exited electrons is relevant. Recently, it has been demonstrated that a hot electron gas that is not in equilibrium with the lattice can induce chemical surface reactions that are inhibited under equilibrium conditions.[4] Accordingly, the relaxation behavior of excited electrons influences the reactivity of an interface and it is therefore important to gain insight how nanostructuring modifies the electron relaxation at interfaces. Here we demonstrate, that time-resolved two-photon photoemission spectroscopy provides a direct probe for the electron energy distribution and, therefore, allows us to investigate the electron relaxation in supported nanoparticles in pump-probe experiments.

Electron-electron, electron-surface, and electron-phonon scattering events determine the relaxation of nonequilibrium electrons in metals. In recent years time-resolved reflection or absorption measurements[5,6] and two-photon photoemission spectroscopy[7–10] were used to investigate the response of the electron gas in bulk metals or thin films directly in the time domain. All these techniques are based on the pump-probe scheme, i.e., a first ultrashort laser pulse excites the system and a second time-delayed laser pulse monitors the effect of the first one. The optical excitation with a laser pulse leads to a transient perturbation of the electron energy distribution $f(E)$. The pure optical methods, i.e., reflection and transmission measurements, indirectly monitor this transient $f(E)$ via the change of the dielectric function $\varepsilon(\omega)$.[11] Therefore, their interpretation is based on linking the nonequilibrium electron distribution to $\varepsilon(\omega)$. In contrast, time-resolved two-photon photoemission spectroscopy reveals directly the occupation of intermediate states and therefore provides energy resolved information on the evolving electron distribution.[7,12]

Time-resolved two-photon photoemission can be extended to the investigation of inhomogeneous surfaces by tuning the laser excitation to a specific resonance. This resonance enhanced two-photon photoemission spectroscopy of an inhomogeneous surface has recently been demonstrated using Ag nanoparticles supported on graphite[13,14] or in larger nanostructures formed by lithography.[15] The nanoparticles on graphite are excited selectively by tuning the wavelength of the laser pulses into the surface plasmon resonance. In contrast to this, two-photon photoemission from mass-selected small Ag_n clusters ($n=2-9$) deposited on graphite occurs via an excitation of the substrate.[16] In case of the resonant excitation of larger nanoparticles investigated here, the total photoemission yield is dominated by the emission from the nanoparticles although the nanoparticles cover only about one percent of the substrate.[13] Here we demonstrate that this dominating photoemission from the nanoparticles allows to probe the transient electron energy distribution in the nanoparticles.

The nanoparticles were prepared following the procedure given in Ref. 17. Cleaved highly oriented pyrolytic graphite (HOPG) is sputtered with Ar^+ ions (1 keV, 10^{11} cm^{-2}) and oxidized in air ($T=520\,°C$, 20 min) thereby forming pits in the topmost layer of the graphite. Silver is evaporated onto the sample (0.1 Å s^{-1}, 10 s, 350 °C), condenses into the pits and forms particles of several nanometers height with an height to diameter ratio larger than 0.6. An *in situ* scanning tunneling microscopy allows us to determine the height distribution of the nanoparticles that exhibits typically a relative width of about 25%. Time-resolved two-photon photoemission spectroscopy is performed using the output of an amplified Ti:sapphire laser system (776 nm, 60 fs pulse duration, repetition rate 100 kHz, focus 30 μm diameter) and its second harmonic (388 nm, 50 fs pulse duration, focus 20 μm diameter) as pump and probe pulses, respectively. For time-resolved studies, pump and probe pulses are delayed with respect to each other. The kinetic energy of the emitted photoelectrons is analyzed using a time-of-flight spectrometer.

The pump-probe scheme is depicted in Fig. 1(a). The irradiation of the sample with an ultrashort laser pulse at 776 nm (1.6 eV) is not resonant with the surface plasmon of the nanoparticles. This leads to the formation of a nonequilibrium electron distribution in substrate and metal nanoparticles as schematically indicated by the steps in the elec-

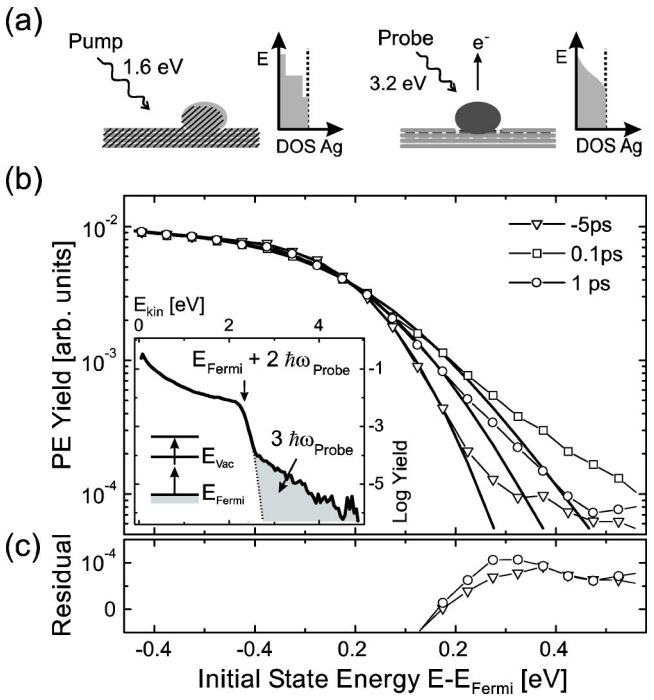

FIG. 1. (a) Scheme of pump- and probe-pulse excitation of supported nanoparticles on graphite. The shaded area in the representation of the silver density of states (dotted lines) indicates the occupation of states. (b) Two-photon photoemission spectra for different pump-probe delays for Ag nanoparticles on graphite (average particle height 4.4 nm) as a function of the initial state energy. The thick solid lines represent best fits to the experimental data using the fitting function explained in the text. The total spectrum for excitation with the probe pulse (3.2 eV, laser fluence 0.1 mJ cm^{-2}) alone is shown in the inset. (c) Difference between experimental spectrum and fit a for delay of -5 ps (triangle) and 1 ps (circle).

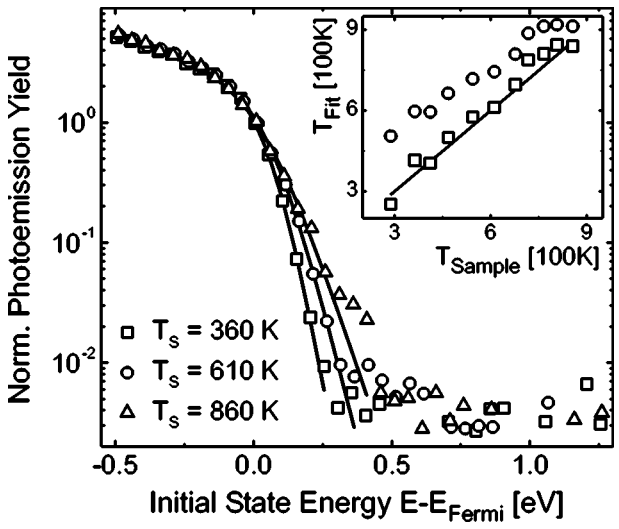

FIG. 2. Two-photon photoemission spectra from Ag nanoparticles on graphite for different sample temperatures. The solid lines represent best fit results using the fitting function described in the text. The relation between the electron gas temperature T_{el} obtained from the fit and the actual sample temperature T_s is shown as inset assuming either infinite spectral resolution (circles) or a constant but finite spectral resolution (squares). The solid line represents a one to one relation.

tron occupation in Fig. 1(a). The probe pulse at 388 nm (3.2 eV) is resonant with the surface plasmon and a two-photon photoemission process leads to the selective photoemission from the Ag nanoparticles. The photoemission spectrum of the probe pulse alone is shown as an inset in Fig. 1(b). The two-photon photoemission contribution reaches up to kinetic electron energies of 2.3 eV, limited by the photoemission from initial states close to E_F. The photoelectrons at kinetic energies above 2.3 eV originate from higher order multiphoton processes. For initial states close to E_F the relative contribution of photoelectrons emitted from the HOPG substrate has been shown to be less than 0.1 %.[13] Photoelectron spectra for three different pump-probe delay times are shown in Fig. 1(b). At negative pump-probe delay, i.e. the probe precedes the pump, the spectrum exhibits a steep slope for initial states close to E_F, reflecting the low temperature of the electron gas. At a delay of 0.1 ps the photoelectron spectrum extends to higher energies and the slope is less steep. With a further increase of the pump-probe delay (1 ps) the steepness increases again and for large delay the original shape of the spectrum is restored. The observed transient shape of the spectrum is in good qualitative agreement with the observations of Fann *et al.* in time resolved two-photon photoemission experiments using a thin Au film.[12] However, the determination of an absolute electron gas temperature from the shape of the spectrum is based on several assumptions, e.g., about the energy distribution of the joint density of states for the optical excitation or the spectrometer transmission.

Therefore, it is crucial to unambiguously link the shape of the spectrum with the electron gas temperature T_{el} by a calibration method. This is achieved by recording spectra at different sample temperatures and relating their shape to the actual sample temperature. Two-photon photoemission spectra are recorded for sample temperatures in the range between 300–900 K. Note that the spectra are recorded at a lower fluence of the 388 nm radiation than the spectra shown in Fig. 1(b) leading to a lower three-photon contribution in the spectra. The higher probe fluence in the time-resolved experiment is chosen to achieve sufficient statistics in the spectra. The slope of the photoelectron spectrum in the vicinity of E_F increases continuously as the sample temperature decreases (Fig. 2). For a quantitative comparison the shape of the spectrum is parametrized by a phenomenological fitting function. For initial state energies close to E_F the shape of the spectrum is modeled by a function consisting of a Fermi function multiplied by an exponential and convoluted with a normal distribution. The temperature dependent Fermi function then directly represents the changing occupation of states and, therefore, the changes of the spectrum with the electron gas temperature T_{el}. The exponential takes into account the spectrometer transmission and the photoemission probability. The convolution with a normal distribution allows for the finite spectrometer resolution and additional spectral broadening mechanisms such as the finite spectral width of the excitation laser pulses. Assuming the absence of spectral broadening the electron gas temperature T_{el} (open

circles in inset in Fig. 2) is higher than the actual sample temperature T_s. With rising T_s, however, the difference between both temperatures becomes smaller. The difference between the experimentally determined T_{el} and the actual sample temperature T_s is attributed to spectral broadening. Adjusting the width of the normal distribution in the fitting function eliminates the difference (open squares in inset in Fig. 2). Note that the broadening parameter is identical for all spectra in the calibration sequence. The good agreement between T_{el} and T_s shows that the shape of the Fermi edge in the spectra is a quantitative measure for T_{el} in Ag nanoparticles on graphite. The result demonstrates that the two-photon probe process conserves the information about the initial state energy and that the shape of the spectrum reflects the electron energy distribution $f(E)$ close to E_F.

Based on this calibration, the spectra shown in Fig. 1(b) are parametrized by fitting the abovementioned function. The best fits for spectra recorded at different pump-probe delays are shown in Fig. 1(b). Up to 0.2 eV above E_F the fit closely follows the experimental data. The good agreement between data and fit shows that $f(E)$ in the vicinity of E_F is again well characterized by an electron gas temperature T_{el}. At higher energy the fit deviates from the spectra because of contributions from three-photon photoemission by the probe pulse and a nonthermal electron distribution generated by the pump pulse. The three-photon contribution generated by the probe pulse is independent of the pump-probe delay and thus can be determined in a spectrum recorded at negative delay as the difference between fit and experimental data [Fig. 1(c)]. During overlap of pump and probe pulse and for a small positive delay the electron distribution differs from a thermal distribution. However, for a positive delay of one ps the difference between experimental spectrum and model fit is identical within the experimental uncertainty with that for negative delay, i.e., the difference results only from the three-photon contribution. This shows that the electron distribution in the nanoparticles is thermalized after 1 ps. Accordingly, the electron gas temperature for larger pump-probe delay is a direct measure of the excess energy stored in the electron gas. In contrast, for a small delay the parameter T_{el} has no distinct physical meaning since the electron distribution is nonthermal.

In principle, it is conceivable that the non-equilibrium between electron gas and lattice, i.e., the different electron gas and lattice temperature, can alter the shape of the photoemission spectrum in comparison to thermal equilibrium conditions. This would introduce a systematic error in the determination of the transient electron gas temperature in the described pump-probe experiment. But as it is shown in the following the effect is negligible within the boundaries given by the experimental uncertainties. The dominating mechanism influencing the spectral resolution is electron-phonon scattering in the intermediate or final state of the probe-pulse photoemission process. An increased lattice temperature, i.e. an increase of the number of phonons, leads to a broadening of the spectral features that depends on the lattice temperature. However, the fact that we can fit all photoemission spectra of the heated sample (Fig. 2) using the identical broadening parameter indicates that this effect is smaller than the experimental uncertainty of the calibration and can therefore be neglected.

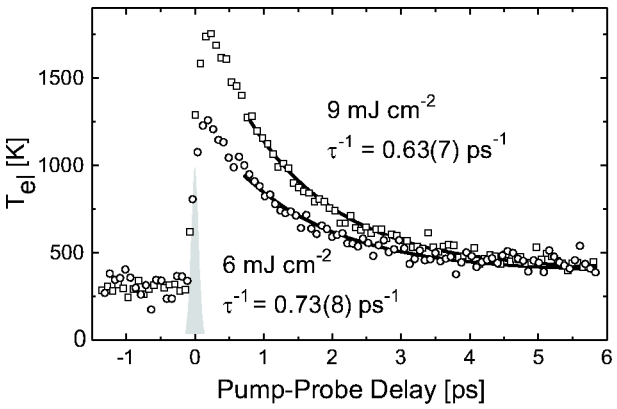

FIG. 3. The transient electron gas temperature T_{el} as it is determined by fitting of the photoemission spectra is shown for two different pump laser fluences. The Ag nanoparticles supported on graphite have an average particle height of 4.4 nm. The cross correlation of pump and probe pulse is shown as shaded area.

The fitting results for the fit parameter T_{el} are shown in Fig. 3 as a function of the pump-probe delay. In coincidence with the pump pulse, T_{el} starts to rise and reaches its maximum at 1200 and 1800 K for 6 and 9 mJ cm^{-2} pump fluence, respectively. The maximum is reached only about 100 to 200 fs after the termination of the pump pulse. It does not reflect the excess energy in the electron gas since the corresponding electron distribution is not yet thermalized. However, the electron distribution for initial states in the energy range between $E_F-0.2$ eV and $E_F+0.2$ eV is well described by the fit parameter T_{el} even for these nonthermal electron distributions. This is interesting with respect to a comparison with transient optical absorption measurements,[18–20] since the transient optical response is primarily sensitive to the largest change in the distribution function, i.e., the change in occupation for states close to the Fermi level. After reaching its maximum T_{el} decreases towards a value slightly above the initial temperature. This reduction of T_{el} is accompanied by the formation of equilibrium between electron gas and lattice. In the following we concentrate on the cooling of the electron gas and therefore we restrict the analysis of the transient temperature to a delay larger than 0.75 ps. Accordingly the obtained T_{el} is a good measure for the excess energy in the electron gas and the determined cooling rate is not influenced by the initial nonthermal electron distribution. The fitting of an exponential to the decay curve of T_{el} yields within the experimental uncertainty identical cooling rates of about 0.7 ps^{-1} for both employed pump fluences.

The cooling rates for differently sized nanoparticles and an Ag(111) crystal are summarized in Fig. 4. The electron gas cooling rate in the nanoparticles is reduced by a factor of about 2 compared to a crystalline Ag(111) surface and shows only a weak increase with particle size in the range between 1.5–4.5 nm particle height. The cooling rate of 1.7 ± 0.4 ps^{-1} for the Ag(111) agrees well with the value 1.4 ± 0.2 ps^{-1} deduced from transient reflection measurements

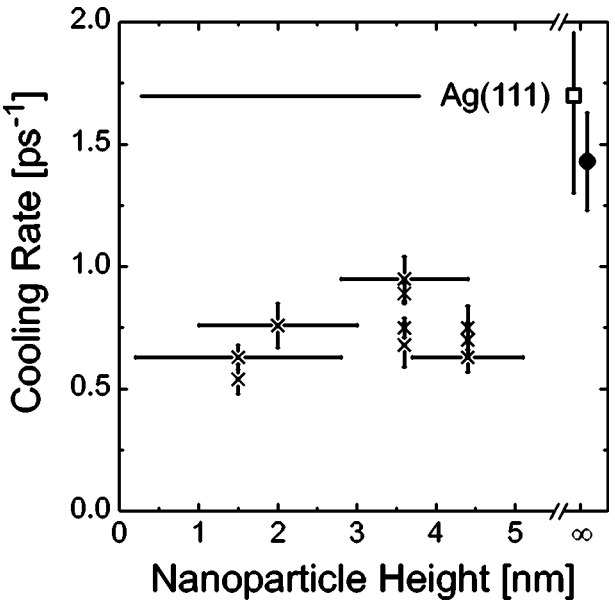

FIG. 4. Electron gas cooling rate for different sized nanoparticles (x) and for a crystalline Ag(111) surface (open square). The different data points for a given average particle height reflect the results from different experiments using the same sample but different pump fluence covering the range $2-16\ \mathrm{mJ\,cm^{-2}}$. The closed circle reflects the cooling rate for a polycrystalline Ag film of 45 nm thickness taken from Ref. 6.

using thin polycrystalline Ag films.[6] Electron relaxation in embedded nanoparticles has been studied by time-resolved absorption experiments (see, e.g., Refs. 18–20). Ag nanoparticles embedded in a glass matrix exhibit an increase of the cooling rate from $1.2-1.8\ \mathrm{ps^{-1}}$ with decreasing size in the range between 10–4 nm diameter.[21] This is in contrast to the reduced cooling rate for supported nanoparticles reported here and we, therefore, conclude that the electron relaxation in supported and embedded nanoparticles differs substantially.

A further discrepancy between embedded and supported nanoparticles appears in the fluence dependence of the electron gas cooling rate. Although, the pump laser fluence varies between $2-16\ \mathrm{mJ\,cm^{-2}}$ in the experiments summarized in Fig. 4, the electron gas cooling rate for supported nanoparticles of about $0.7\ \mathrm{ps^{-1}}$ is constant within the experimental uncertainties. The corresponding maximum temperature rise of T_{el} varies between 400 to 1600 K. However, according to the experiments using embedded nanoparticles[22] or the predictions of the two temperature model (TTM)[23] a fluence dependence of the cooling rate is expected. This discrepancy indicates, that the electron relaxation in supported nanoparticles cannot be treated using the TTM for a homogeneous system. We attribute this to the fact that the TTM treats only the energy exchange between electron gas and lattice and does not take into account the transport of energy between nanoparticle and substrate. On a short time-scale in particular, the transport of excited electrons between nanoparticle and substrate influences the balance of energy in the nanoparticles. This process is determined by the interface between substrate and nanoparticle and therefore can account for the vanishing size dependence of the cooling rate seen in our experiments.

Summarizing, the resonant excitation of the surface plasmon in Ag nanoparticles and the associated enhancement of the two-photon photoemission from the nanoparticles allows us to monitor the transient electron energy distribution in the nanoparticles in time-resolved pump-probe experiments. The spectral shape of the photoelectron spectrum together with a temperature calibration obtained at different sample temperatures provide a quantitative measure for the transient electron gas temperature. In contrast to transient absorption spectroscopy, that relies on a model dielectric function to extract the transient T_{el}, the two-photon photoemission spectrum is a direct measure of the electron energy distribution in the Ag nanoparticles. The time resolved experiments exhibit an electron gas cooling rate for supported Ag nanoparticles of about $0.7\ \mathrm{ps^{-1}}$. It is reduced by a factor of 2 in comparison to bulk silver and shows only a weak size dependence (in the range from 1.5 to 4.5 nm height). The reduced cooling rate and the fact that it exhibits no significant fluence dependence ($2-16\ \mathrm{mJ\,cm^{-2}}$) deviates from the behavior of embedded nanoparticles that has been reported in literature. We attribute this to the different role of energy transport between substrate and nanoparticle. In future experiments time-resolved experiments for nanoparticles on different substrates, e.g., thin oxide layers,[24] will allow us to investigate the influence of excited electron transport between nanoparticle and substrate. Furthermore, in the present work the transient electron distribution is reduced to a single parameter, i.e., the electron gas temperature. However, the transient spectral shape also contains information about the thermalization of the initial nonthermal electron energy distribution. Based on a suitable model for electron relaxation in an inhomogeneous system, which is currently developed, this information can be extracted from the experimental data.

[1] G. Ertl and H. J. Freund, Phys. Today **52/1**, 32 (1999).
[2] M. Valden, X. Lai, and D. W. Goodman, Science **281**, 1647 (1998).
[3] A. Sanchez, S. Abbet, U. Heiz, W. D. Schneider, H. Hakkinen, R. N. Barnett, and U. Landman, J. Phys. Chem. A **103**, 9573 (1999).
[4] M. Bonn, S. Funk, C. Hess, D. N. Denzler, C. Stampfl, M. Scheffler, M. Wolf, and G. Ertl, Science **285**, 1042 (1999).
[5] C. K. Sun, F. Vallee, L. Acioli, E. P. Ippen, and J. G. Fujimoto, Phys. Rev. B **48**, 12 365 (1993).
[6] R. H. M. Groeneveld, R. Sprik, and A. Lagendijk, Phys. Rev. B **51**, 11 433 (1995).
[7] W. S. Fann, R. Storz, H. W. K. Tom, and J. Bokor, Phys. Rev. Lett. **68**, 2834 (1992).
[8] M. Aeschlimann, S. Pawlik, and M. Bauer, Ber. Bunsenges. Phys. Chem. **99**, 1504 (1995).

[9] H. Petek and S. Ogawa, Prog. Surf. Sci. **56**, 239 (1997).
[10] E. Knoesel, A. Hotzel, and M. Wolf, Phys. Rev. B **57**, 12 812 (1998).
[11] C. K. Sun, F. Vallee, L. H. Acioli, E. P. Ippen, and J. G. Fujimoto, Phys. Rev. B **50**, 15 337 (1994).
[12] W. S. Fann, R. Storz, H. W. K. Tom, and J. Bokor, Phys. Rev. B **46**, 13592 (1992).
[13] J. Lehmann, M. Merschdorf, W. Pfeiffer, A. Thon, S. Voll, and G. Gerber, Phys. Rev. Lett. **85**, 2921 (2000).
[14] M. Merschdorf, W. Pfeiffer, A. Thon, S. Voll, and G. Gerber, Appl. Phys. A: Mater. Sci. Process. **71**, 547 (2000).
[15] M. Scharte, R. Porath, T. Ohms, M. Aeschlimann, J. R. Krenn, H. Ditlbacher, F. R. Aussenegg, and A. Liebsch, Appl. Phys. B: Lasers Opt. **73**, 305 (2001).
[16] U. Busolt, E. Cottancin, H. Rohr, L. Socaciu, T. Leisner, and L. Wöste, Appl. Phys. B: Lasers Opt. **68**, 453 (1999).
[17] H. Hövel, T. Becker, A. Bettac, B. Reihl, M. Tschudy, and E. J. Williams, J. Appl. Phys. **81**, 154 (1997).
[18] J. Y. Bigot, V. Halte, J. C. Merle, and A. Daunois, Chem. Phys. **251**, 181 (2000).
[19] S. Link and M. A. El Sayed, Int. Rev. Phys. Chem. **19**, 409 (2000).
[20] C. Voisin, N. Del Fatti, D. Christofilos, and F. Vallee, J. Phys. Chem. B **105**, 2264 (2001).
[21] N. Del Fatti, C. Flytzanis, and F. Vallee, Appl. Phys. B: Lasers Opt. **68**, 433 (1999).
[22] N. Del Fatti, C. Voisin, M. Achermann, S. Tzortzakis, D. Christofilos, and F. Vallee, Phys. Rev. B **61**, 16956 (2000).
[23] M. I. Kaganov, I. M. Lifshitz, and L. V. Tanatarov, JETP Lett. **4**, 173 (1957).
[24] M. Bäumer and H. J. Freund, Prog. Surf. Sci. **61**, 127 (1999).